

# Learning Dynamics from Kinematics: Estimating Foot Pressure from Video

Christopher Funk<sup>\*†</sup>, Savinay Nagendra<sup>\*†</sup>, Jesse Scott<sup>†</sup>, John H. Challis<sup>§</sup>, Robert T. Collins<sup>†</sup>, Yanxi Liu<sup>†</sup>

<sup>†</sup>School of Electrical Engineering and Computer Science. <sup>§</sup>Biomechanics Laboratory.  
The Pennsylvania State University. University Park, PA. 16802, USA

funk@cse.psu.edu, sxn265@psu.edu, jescott@cse.psu.edu, jhc10@psu.edu, rcollins@cse.psu.edu, yanxi@cse.psu.edu

## Abstract

Human pose stability analysis is the key to understanding locomotion and control of body equilibrium, with numerous applications in the fields of kinesiology, medicine and robotics. We propose and validate a novel approach to learn dynamics from kinematics of a human body to aid stability analysis. More specifically, we propose an end-to-end deep learning architecture to regress foot pressure from a human pose derived from video. We have collected and utilized a set of long (5min+) choreographed Taiji (Tai Chi) sequences of multiple subjects with synchronized motion capture, foot pressure and video data. The derived human pose data and corresponding foot pressure maps are used jointly in training a convolutional neural network with residual architecture, named PressNET. Cross-validation results show promising performance of PressNET, significantly outperforming the baseline method under reasonable sensor noise ranges. We also show that the center of pressure locations computed from our regressed foot pressure maps are more accurate than those obtained from the baseline approach.

## 1. Introduction

In the realm of health and sports, precise and quantitative digital recording and analysis of human motion provide rich content for performance characterization and training, cross-sectional/longitudinal health status assessment and diagnosis or even preventive therapy of neurodegenerative syndromes. In recent years, gait analysis and control/balance of equilibrium has received an increasing interest from the research community [39, 40, 54]. This is mainly due to the necessity of understanding the complex mechanisms of the human postural system, which con-

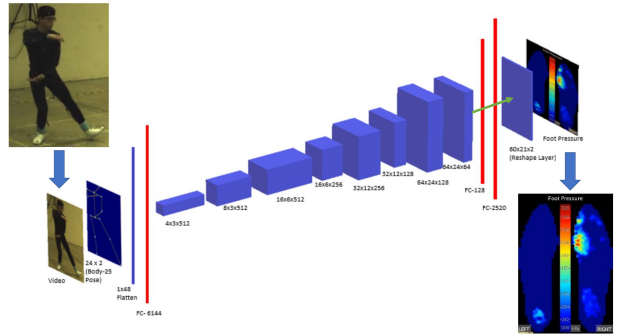


Figure 1: Our PressNET networks learn to predict a foot pressure heatmap from video based on estimating Body-25 joints from a video frame using OpenPose and then regressing directly to 2D foot pressure. The green line signifies a concurrent branch around the fully connected layers (only for PressNET-V2).

tribute to the development of efficient solutions for unstable postures in terms of orientation and equilibrium. Stability analysis has a wide number of applications in the fields of Health care, Kinesiology and Robotics, aiming to understand locomotion and duplicate human body movements during numerous physical activities. Understanding body dynamics, such as foot pressure, is essential to study the effects of perturbations caused by external forces and torques on the human postural system, which changes body equilibrium in static posture as well as during locomotion.

Current computer vision research focuses mainly on extracting skeletal kinematics from videos, using body pose estimation and tracking to infer an estimate of skeletal pose and joint angles in each frame as well as the movement of body and limbs over time [3, 8, 9, 11, 12, 17, 35, 49]. However, little has been investigated on whether quantitative dynamics information can be inferred from a single video of a person’s movement. While body joints and their degrees of freedom constrain the types of motion, it is the properties and actions of the muscles and weight distributions,

\* Contributed equally, order chosen alphabetically

i.e. body dynamics, that dictate the range of motion, speed and feasible poses produced with these degrees of freedom. Consideration of human body dynamics has been successful in explaining performance in athletics activities, for example the triple jump [2], and vertical jump performance [15]. Similarly, analysis of dynamics has been used to show that strength is the limiting factor in the ability of the elderly to rise from a chair [27], and to determine the causes of stiff-knee gait in subjects with cerebral palsy [20]. We believe an effective analysis of human movement must take into account the the dynamics of the human body, and we ask the question: Can human motion dynamics be inferred from video sensors that are incapable of observing muscle activations, physical loads and external forces directly?

This paper explores a deep learning approach to transform kinematics (body pose) to dynamics (foot pressure). In order to achieve this goal, we have created the largest dataset, with over 350k frames, of synchronized video and foot pressures. We represent foot pressure by an intensity heatmap that provides the distribution of pressure applied by different points of the foot against the ground, measured in kilo Pascals (kPa) over discretized foot sole locations. The body pose is represented in terms of human joint locations, extracted from videos of subjects performing choreographed Taiji (Tai Chi) sequences by applying the Openpose [9] Body-25 model on the video frames. For training data, we record video data and foot pressure maps synchronously so that there is a foot pressure map of both feet corresponding to each video frame. This is used as training data to train two versions of a deep convolutional neural network residual architecture (Figure 1) to regress foot pressure heatmaps from a given body pose. We perform a leave-one-out cross subject evaluation over the data of five subjects using our network. K-Nearest Neighbors (KNN) is applied to establish a baseline for each of the five cross-subject splits. Mean absolute error is used to evaluate the performance of the networks. Our results show that the network outperforms KNN across all the five splits.

We have chosen 24-form simplified *Taiji Quan* (Taiji or Tai Chi) [52] as a testbed for validating computer vision algorithms. Taiji was selected because it is low-cost, hands-free, and slow while containing complex body poses and movements in all orientations. Taiji is practiced worldwide by millions of people of all gender, race, and ages. The routines last about 5 minutes and consist of controlled choreographed movements where the subject attempts to remain balanced the entire time.

We present a method to predict foot pressure heatmaps directly from video alone and the major contributions of this paper are:

- creating the largest synchronized video and foot pressure dataset ever recorded for Taiji and
- presenting a novel deep architecture, PressNET, which

is the first network to regress dynamics (foot pressure) of a subject directly from kinematics (human pose), aiding in human motion stability analysis.

## 2. Related Work

After the introduction of Deep Pose by Toshev *et al.* [49], there was a paradigm shift in the field of human pose estimation from classical approaches to deep networks. The idea of using heatmaps for visualization as well as for use as ground truth data in a regression problem was introduced for the first time by Tompson *et al.* [48]. Stacked hour glass networks by Newell *et al.* [35] gave state of the art results for pose estimation using heat map regression with a bottom-up top-down approach. They use the network based off Tompson *et al.*, where convolution layers are used jointly with a graphical model to learn spatial relationships between joints and other human pose estimators [3, 8, 9, 11, 12, 17, 35, 49]. This was the first network to successfully implement a pose estimator using residual convolution layers for additional spatial processing at different resolutions. Encoder-Decoder architectures have been predominantly used for human pose estimation. An hourglass network, before stacking, is also similar to an encoder-decoder architecture, where skip connections help in preserving spatial coherence at each scale [19]. Having deep residual/skip connections to preserve spatial information across multiple resolutions through the network is essential for unsupervised/semi-supervised feature learning [26]. Densely connected convolutional networks have achieved state of the art accuracies by using residual feed forward connections between convolution layers.

Success in 2D human pose estimations has encouraged researchers to detect 3D skeletons from image/video by extending the existing 2D human pose detectors [7, 10, 31, 32, 36, 43] or by directly using the image features [1, 38, 41, 44, 56]. State-of-the-art methods for 3D human pose estimation from 2D images have concentrated on deep systems. Tome *et al.* [46] proposed an estimator that reasons about 2D and 3D estimation to improve both tasks. Zhou *et al.* [55] augmented a 2D estimator with a 3D depth regression sub-network. Martinez *et al.* [31] showed that given high-quality 2D joint information, the process of lifting 2D pose to 3D pose can be done efficiently using a relatively simple deep feed-forward network.

Until now all the papers discussed concentrate on pose estimation from 2D images or depth maps. These papers concentrate on learning joint angles or joint locations, which can be broadly classified as learning a very basic type of kinematics for a whole body skeleton. These methods do not delve into the external torques/forces exerted by the environment which lead to a change in balance or physical interaction of the body with the scene.

There have been many studies on human gait analy-

sis [4, 16, 29, 30] using qualitative approaches. Grimm *et al.* [22] aimed to predict the pose of a patient using foot pressure mats. Liu *et al.* [30] used frieze patterns to analyze gait sequences. Although these are some insightful ways to analyze gait stability, there has been no deep learning approach to tackle this problem. In this paper, we aim to use a body’s kinematics to predict its dynamics and hence develop a quantitative method to analyze human stability analysis using foot pressure.

### 3. Our Approach

#### 3.1. Data Collection

Three modes of data - Video, Motion Capture and Foot Pressure - are recorded simultaneously for five subjects performing choreographed 24-Form Taiji-Quan sequences. Each session consists of three performances by the subject wearing motion capture markers and insole foot pressure measurement sensors. Vicon Nexus software is used to synchronize motion capture and video data spatiotemporally, while Tekscan F-scan foot pressure sensor measurements are synchronized post collection. This is the first dataset to record synchronized video, motion capture and foot pressure data.

##### 3.1.1 Video

Raw video data is processed using the Nexus software to trans-code it to a compressed video, with each video having its own spatiotemporal calibration. Human pose is predicted on the compressed video using OpenPose [9]. OpenPose uses non-parametric representations, referred to as Part Affinity Fields, to regress joint positions as well as connections between the joints. We use the maximum accuracy configuration of the network to extract Body-25 joints from videos. Each detected key-point has a confidence associated with it, which estimates the accuracy of prediction of a particular joint location. The output from OpenPose network thus has 3 channels, (X, Y, confidence), denoting the X and Y pixel coordinates and confidence of prediction for each of the 25 joints, making it of size  $(25 \times 3)$ .

Figure 2 shows the body-25 skeleton. The 25 keypoints are: {0:Nose, 1:Neck, 2:RShoulder, 3:RElbow, 4:RWrist, 5:LShoulder, 6:LElbow, 7:LWrist, 8:MidHip, 9:RHip, 10:RKnee, 11:RAnkle, 12:LHip, 13:LKnee, 14:LAnkle, 15:REye, 16:LEye, 17:REar, 18:LEar, 19:LBigToe, 20:LSmallToe, 21:LHeel, 22:RBigToe, 23:RSmallToe, 24:RHeel} The video frames of a subject performing Tai Chi, as shown in Figure 2 are processed through the OpenPose network to extract the 25 body joint locations with respect to a fixed coordinate axis. For the purpose of visualization, 2D Gaussian heatmaps are drawn over the joint locations, with the peak of each Gaussian corresponding to

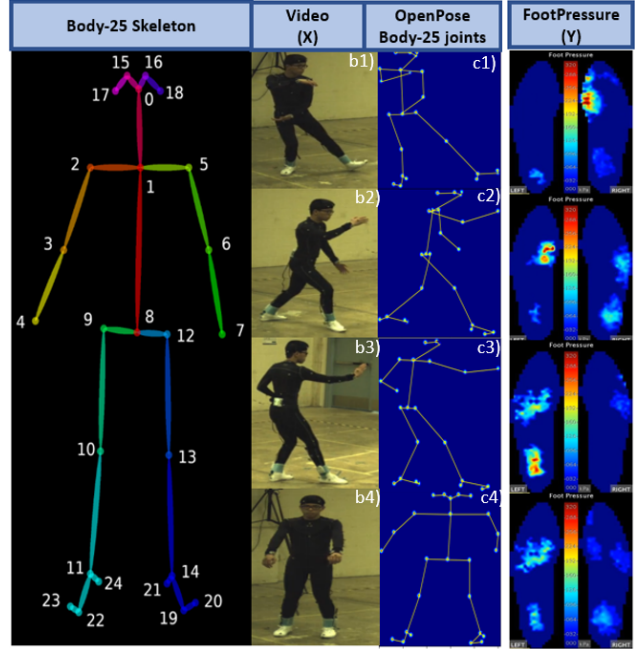


Figure 2: Left: Body-25 joint set labeled by Openpose. Middle: The video data and the corresponding Openpose detections showing the detected skeletons with Gaussian distributions over each joint. The 2D position of these joints are used as the input to the PressNETs. Right: The corresponding foot pressure maps.

the confidence of detection of that joint, as shown in Figure 2. The confidence of keypoints 15 to 18 are zero for more than 50% of the video frames due to occlusions. However, these keypoints are still given as inputs to our network. The reason for this is as follows: We are trying to establish a correlation between the 25 key points and the corresponding foot pressures where we want our network to learn the factor of usability of each key point in predicting the foot pressure without prior assumptions as to which key points might be necessary in the regression task. Eventually, the network learns to discard the zero confidence key points to avoid affecting the accuracy of prediction.

##### 3.1.2 Foot Pressure

Foot pressure is collected using a Tekscan F-Scan insole pressure measurement system. Each subject is provided a pair of canvas shoes outfitted with cut to fit capacitive pressure measurement insoles that have a maximum width of 21 *prexels* (pressure pixels) and a maximum height of 60 *prexels* with a total of approximately 900-1,000 pressure *prexels* per frame depending on shoe size. These two insole sensors are recorded through a battery operated wearable recording system. The data is recorded with a noise floor of approximately 3kPa.

During each session, the subject follows an integrated

Subject	Session	Take	# frames	Foot Pressure Statistics (kilo Pascals)					Total # frames
				Mean	Std	Median	Max	Min	
Subject-4	1	1	9,595	6.52	10.62	1.99	73.12	0	99,609
		2	14,364	6.24	10.16	1.91	74.32	0	
		3	2,412	5.94	8.94	2.67	55.33	0	
	2	1	14,248	7.74	12.866	2.27	99.57	0	
		2	13,460	8.41	14.28	2.33	110.95	0	
		3	13,255	8.87	15.13	2.29	117.92	0	
	3	1	5,917	6.47	10.46	2.16	63.78	0	
		2	13,106	6.38	11.22	1.86	88.36	0	
		3	13,252	6.44	11.05	1.87	78.64	0	
Subject-7	1	1	18,000	3.37	4.72	2.4	31.33	0	158,920
		2	17,626	3.47	4.45	2.18	28.5	0	
		3	17,702	3.29	4.27	2.08	28.98	0	
	2	1	17,706	6.18	8.09	3.79	56.95	0	
		2	17,354	5.76	7.74	3.53	55.47	0	
		3	17,625	5.42	7.43	3.25	53.85	0	
	3	1	17,576	5.4	8.04	2.98	62.45	0	
		2	17,645	5.39	7.94	3.09	62.4	0	
		3	17,686	5.35	8.12	2.91	62.07	0	
Subject-8	2	1	14,103	5.26	11.84	0.069	99.05	0	19,702
	3	1	5,599	2.94	7.43	0.027	56.15	0	
Subject-9	1	1	11,211	4.4	6.942	1.37	51.52	0	34,915
	2	1	11,294	6.15	11.19	1.34	89.93	0	
	3	1	12,410	5.78	11.91	0.96	106.18	0	
Subject-10	1	1	13,064	7.35	11.07	2.53	82.68	0	41,871
	2	1	14,500	8.27	14.39	1.94	125.97	0	
	3	1	14,307	8.04	14.82	1.2	124.07	0	

Table 1: Data statistics showing number of video frames per take and session for each subject.

calibration process that determines a linear (scale and offset) calibration for all active prexels of each foot sensor. Each take is recorded as a  $\approx 36,000$  sample series (100 Hz for  $\approx 6$  minutes) and then downloaded at the end of the session. Each take of the raw foot pressure data is subject to issues including non-responsive (bad) prexels and measurement noise. To mitigate these issues, an  $11 \times 1$  median filter is applied temporally to remove impulse noise, and a  $3 \times 3$  filter (or  $5 \times 3$  filter for bad prexel regions  $> 1 \times 1$ ) is used within each frame to remove spatial noise. The foot pressure heatmaps generated are 2 channel images of size  $60 \times 21$ . Figure 2 shows an example of left and right foot pressure visualized with a color mapping (left) and registered into the spatial coordinates of the motion capture system (right).

### 3.1.3 Data Statistics

Data from five subjects performing choreographed sequences of 24-Form Taiji Quan sequences is used for all experiments in this paper. The dataset contains over 350k pairs of video and foot pressure frames. The five subjects are indexed as : ‘Subject-4’, ‘Subject-7’, ‘Subject-8’, ‘Subject-9’ and ‘Subject-10’. The mean, median, standard deviation, maximum and minimum foot pressure values in kilo pascals for each take are shown in Table 1. For cross-validation, data sets are split using a leave-one-out strategy as shown in Table 2. We use all available data for each subject which consists of nine takes of subjects 4 and 7 three takes for subject 8, 9 and 10. Different amounts of data was recorded and available for each subject based on data collection protocols and subject availability. While this does create an imbalance among the subjects in our dataset, this

does not appear to affect the results.

## 3.2. Network and Training

The design of our network is motivated by the residual generator of the Improved Wasserstein GAN [23]. We are using a generator inspired architecture since our input is 1D, converted to a 2D heatmap. This design aids in capturing information at different resolutions, acting like a decoder network for feature extraction. The primary aim of our network is to extract features without loss of spatial information across different resolutions. We try to learn the correlation between the pose encoded in terms of 25 joint locations and the corresponding foot pressure intensity distribution. We train a convolutional residual architecture over data from multiple subjects to regress foot pressure distributions given a pose. We do not use a discriminator since ground truth data is available thus this is a supervised learning problem.

### 3.2.1 Data Pre-processing

Input pose data is centered around the hip joint to aid the network in generalizing to different subjects and to remove camera specific constraints of video recording. The hip joint, which is  $(0, 0)$  after centering, is removed from the training and testing data sets. Data is normalized per-feature by subtracting the feature’s mean and dividing by its standard deviation. Zero confidence (undetected) OpenPose joints are not considered.

Foot pressure data, which is originally recorded in kilo Pascals (kPa) has invalid prexels representing regions outside the footmask marked as Not a Number (NaN). These prexels are converted to since the network library cannot train with NaN values. Any prexel values greater than 1000 kilopascals are clipped to 1000 to remove noise from the dataset. The data is converted to Mega Pascals by dividing by 1000, so that the intensities are in the range  $[0, 1]$ .

## 3.3. Network

The PressNET network is a feed forward convolutional neural network which inputs a 1D vector of joints and outputs a 2D foot pressure (Figure 1). The input layer is a flattened vector of joint coordinates of size  $48 \times 1$ , (24 joints  $\times 2$  coordinates since the hip joint is removed), which contains the kinematic information about a pose. The input is processed through a fully connected layer with an output dimension of  $6144 \times 1$ . This output is reshaped into an image of size  $4 \times 3$  with 512 channels. The network contains four residual convolution blocks (Figure 3 Left), which perform nearest neighbor upsampling. The first block upsamples the input by  $(2, 1)$  and the other three upsample by 2. Each block has two convolution layers of kernel size  $3 \times 3$ . The input to each block is also passed through a  $1 \times 1$  con-

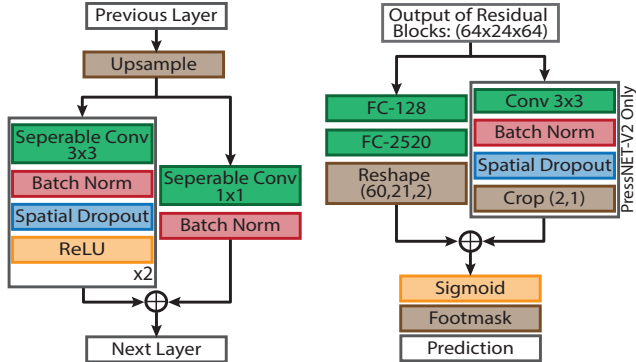


Figure 3: **Left:** A residual block, one of the building blocks of our network, upsamples the data and computes features. **Right:** Final set of layers of our network include a fully connected layer (leftmost path) for both PressNETs and a concurrent branch (rightmost path) in PressNET-V2 to preserve spatial consistency.

volution block and added as a residual connection to the output of the block. All convolutional layers are separable convolution layers that split a kernel into two to perform depth-wise and point-wise convolutions. Separable convolutions reduce the number of network parameters as well as increase the accuracy [13]. Batch normalization [28] and spatial dropouts [47] are applied after every convolution layer. ReLU [34] is used as a common activation function throughout the network, except the output layer. The number of channels of each residual block is progressively halved as the resolution doubles, starting at 512 channels and decreasing to 64. The output of the final residual block is flattened and fed into a fully connected layer FC-128 and FC-2520 and reshaped into the same size as the foot pressure frame (60x21x2). This network processes 1D-2D-1D, where the residual blocks work as feature extractors and the features are fed into fully connected layers. Finally, a sigmoid activation is used to compress the output into a range of [0,1]. We call this architecture “PressNET-V1”.

Another variant, “PressNET-V2”, has a concurrent branch around FC-2520 as shown in Figure 3 Right. The final output from the last residual block is passed into a  $3 \times 3$  normal convolution layer to get a 2 channel output of shape  $64 \times 24$ , as well as into the fully connected branch. This output is further cropped to obtain a two-channeled image of shape  $60 \times 21 \times 2$ , which is the shape of the foot pressure heatmaps. This output is added to the final FC-2520 layer as a residual connection to preserve spatial coherence even after passing through flattening and fully connected layers. The last fully connected layer for both PressNETs has a field of view over the entire prediction and, when combined with the spatial coherence of the concurrent branch for PressNET-V2, yields the best results.

Test Subject	Training Set	Validation Set	Test Set
4	206,406	50,002	99,609
7	213,051	45,568	158,920
8	277,660	57,655	19,702
9	269,258	508,44	34,915
10	264,199	48,947	41,871

Table 2: The number of frames in each split of the data.

### 3.3.1 Training Details

We evaluate the two varieties of our network on five splits of the dataset. Our dataset is split by subject in a leave-one-out cross-validation. The validation data consists of the last take from each subject used in the training data. The number of frames per take are listed in Table 1. The goal of this cross-subject validation is to show how well this network generalizes to an unseen individual. Both networks are trained with a learning rate of  $5e^{-5}$  for 20 epochs at a batch size of 32 for all splits on a NVIDIA Tesla P100 GPU cluster with 8GB of memory. Data pre-processing is carried out before training as mentioned in Section 3.2.1.

Both PressNET-V1 and PressNET-V2 take 3 to 3.5 hours to train on splits with test subjects 8, 9 and 10 and 2 to 2.5 hours to train on splits with test subjects 4 and 7. The problem is formulated as a regression with a sigmoid activation layer as the last activation layer since the output data is in the range [0, 1]. A binary footmask, produced by the foot pressure capturing system, is element-wise multiplied in the network having ones marked for valid prexels and zeros marked for invalid prexels. This enables the network to not have to learn the approximate shape of the foot in the course of training and solely learn foot pressure. The learning rate is reduced to  $1e^{-5}$  after 12 epochs to ensure a decrease in validation loss with training. Mean absolute error is used as the loss function for supervision, as we are learning the distribution of prexels [6].

## 4. Results

We evaluate PressNET qualitatively and quantitatively, as well as compare against a K-nearest neighbor baseline to show that PressNET is effective at estimating foot pressure from input video.

### KNN Baseline

We employ K-Nearest Neighbor (KNN) regression [6] as a baseline. For the KNN regression, the data is temporally subsampled by a factor of 2. This is done to decrease the search time required for the KNN algorithm, without much information loss. The foot pressure data is sampled at 100Hz, i.e., we have a frame of foot pressure recorded

every 10 milliseconds. Since the data is sequential, picking every other frame of training data does not affect the temporal consistency of foot pressure data as the change in the heatmaps in 20 milliseconds is negligible. Pre-processing is carried out similar to training PressNET. The data is normalized by mean and standard deviation of input, calculated using hip joint centered data by ignoring zero confidence values. The distance metric for the KNN algorithm is calculated as the mean of the distances between corresponding joints that do not have zero confidence values. This distance  $d$  can be represented for two OpenPose human pose detections ( $a$  and  $b$ ) with confidence  $c^a$  for  $a$  and  $c^b$  for  $b$  and  $J$  joints by:

$$d(a, b) = \frac{\sum_{j \in J} \|(a_j - b_j)\|_2^2 * \delta(c_j^a c_j^b > 0)}{\sum_{j \in J} \delta(c_j^a c_j^b > 0) + \epsilon} \quad (1)$$

where  $\delta$  is the Kronecker Delta which is 1 if the argument is true and 0 if false and a small  $\epsilon$  to avoid division by 0. This enables KNN to adapt to missing joint detections in the human pose predictions.

#### 4.1. Quantitative Evaluation

For the quantitative evaluation, we use mean absolute error  $E$  to quantify the difference between ground truth foot pressure  $Y$  and predicted foot pressure  $\hat{Y}$  on  $N$  foot pressure prexels as:

$$E = \frac{1}{|N|} \sum_{n \in N} |Y_n - \hat{Y}_n| \quad (2)$$

We then take the mean across all the cross-validation splits for our final accuracy rates.

Table 3 shows the error for our PressNET and the KNN error for the predicted foot pressure for each data split. For both PressNETs, the worst two individuals to predict foot pressure on are Subjects 4 and 10. This is also true for the nearest neighbor classifiers as well which could be because these subject foot pressures have a higher mean foot pressure than the other subjects and thus the networks are under-predicting the error. The PressNET V2 has a mean classification of 5.61 kPa which is less than double the 3 kPa measurement noise level of the foot pressure recording devices.

In order to test whether these results are significant, we perform a two tailed paired t-test between the mean errors for each frame for each of the PressNETs compared with KNN over each split of the data. As shown in Table 4, both networks perform significantly better than KNN regression.

#### 4.2. Qualitative Evaluation

Figure 4 shows the foot pressure predictions for different frames from multiple subjects. In addition to the qualitative comparison by visualization, the respective mean absolute

KNN		Testing Mean Absolute Errors (kPa)			
Test Subject	Mean	Std	Median	Max	Min
4	11.37	2.67	9.95	23.92	3.91
7	9.97	2.4	8.97	22.6	3.007
8	9.73	2.6	8.8	19.21	3.08
9	9.95	2.89	9.32	23.12	2.86
10	11.43	3.08	10.01	25.01	3.51
Means	10.49	2.73	9.41	22.78	3.28
PressNET V1		Testing Mean Absolute Errors (kPa)			
Test Subject	Mean	Std	Median	Max	Min
4	8.22	2.12	8.08	19.43	2.38
7	5.47	1.78	5.21	19.28	2.18
8	5.74	2.13	5.51	18.32	0.82
9	5.59	1.87	5.23	17.16	1.28
10	8.76	2.31	8.38	22.22	3.47
Means	6.76	2.04	6.48	19.28	2.02
PressNET V2		Testing Mean Absolute Errors (kPa)			
Test Subject	Mean	Std	Median	Max	Min
4	6.97	1.97	6.85	18.02	2.39
7	4.67	1.86	4.37	17.29	2.3
8	4.63	2.03	4.46	17.1	0.69
9	4.6	1.907	4.24	19.15	1.19
10	7.21	2.28	7.35	21.06	3.165
Means	<b>5.61</b>	<b>2.009</b>	<b>5.45</b>	<b>18.52</b>	<b>1.94</b>

Table 3: Results for KNN and PressNET V1 and V2 showing the mean absolute error for each split of the data and the mean among the splits. For every statistic, PressNET V2 has the lowest error out of all the regressions tested. The lowest mean values are shown in bold.

Test Subject	PressNET-V1		PressNET-V2	
	t-statistic	P-value	t-statistic	P-value
4	298.19	0	352.13	0
7	597.7	0	548.53	0
8	178.69	0	191.75	0
9	261.84	0	260.87	0
10	106.76	0	111.55	0

Table 4: Paired t-test between Mean Absolute errors of all frames between PressNET-V1, PressNET-V2 and KNN

errors with respect to ground truth frames have also been calculated to provide a quantitative comparison of performance of the three networks. The frames have been chosen to show the ability of PressNET to generalize to different poses, similar poses from different subjects and different views with respect to a fixed camera. The frames have also been chosen to show some failure cases of PressNET.

Observing the foot pressure heatmaps in columns of KNN, PressNET-V1 and PressNET-V2, it is evident that the heatmaps generated by PressNET-V2 are more similar to ground truth heatmaps when compared to the other two.

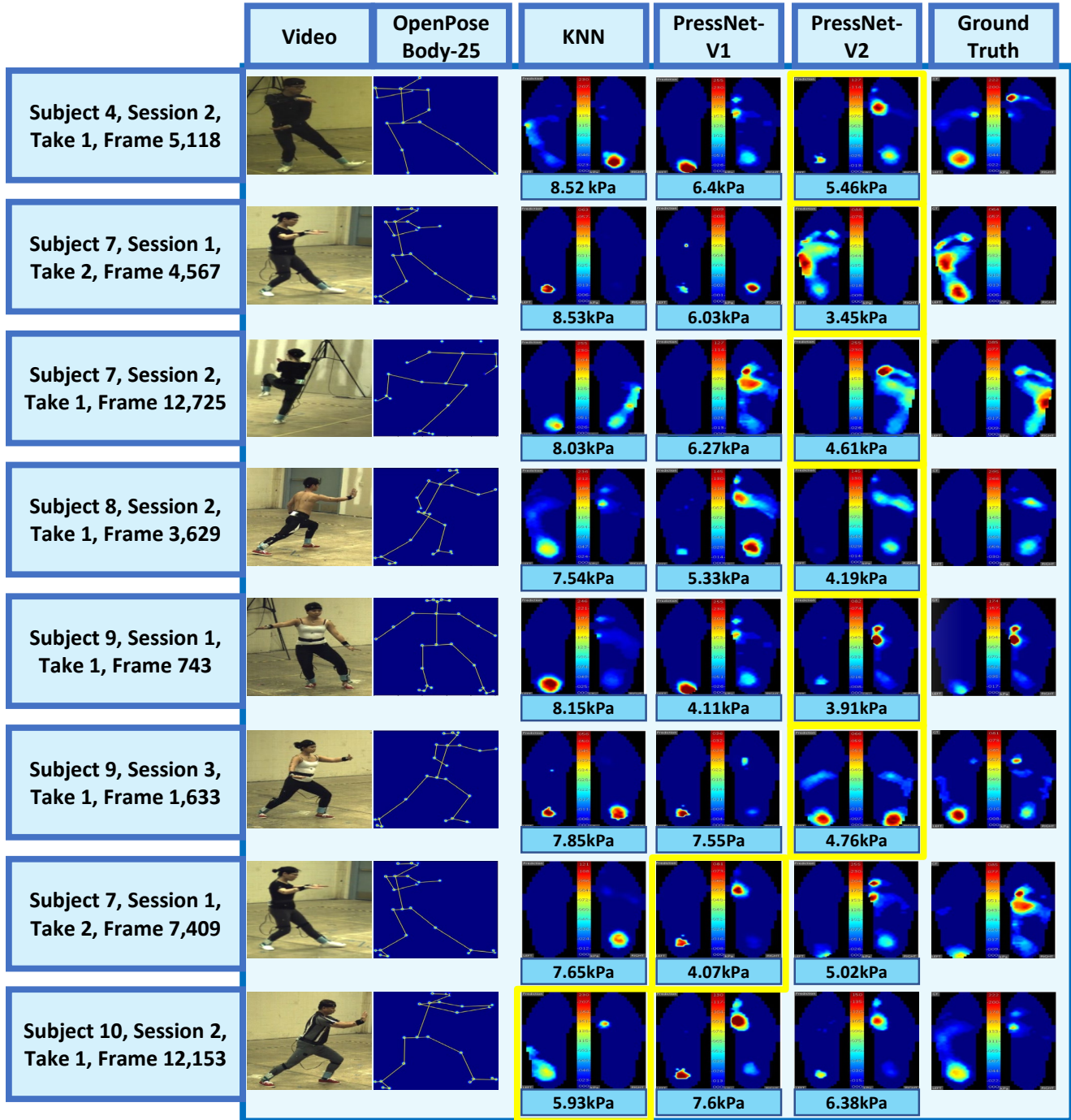


Figure 4: Qualitative results showing (Left to Right): Input data, foot pressure predictions from KNN, PressNET-V1 and PressNET-V2, and ground truth. The foot pressure prediction with the lowest mean absolute error is shown with a yellow rectangle around it.

This is supported by the mean absolute frame errors of the networks. KNN results are visually very poor when compared to the two PressNETs. This is because KNN is merely picking the frame with the shortest distance between joints in a cross-subject evaluation. As the style of performance

and body dynamics differs for each subject, KNN is unable to generalize to a change in subjects, leading to the highest mean absolute error among the three.

Different poses can lead to the same foot pressure. Consider Frames 5118 of Subject 4, Session 2 (first row), Take 1

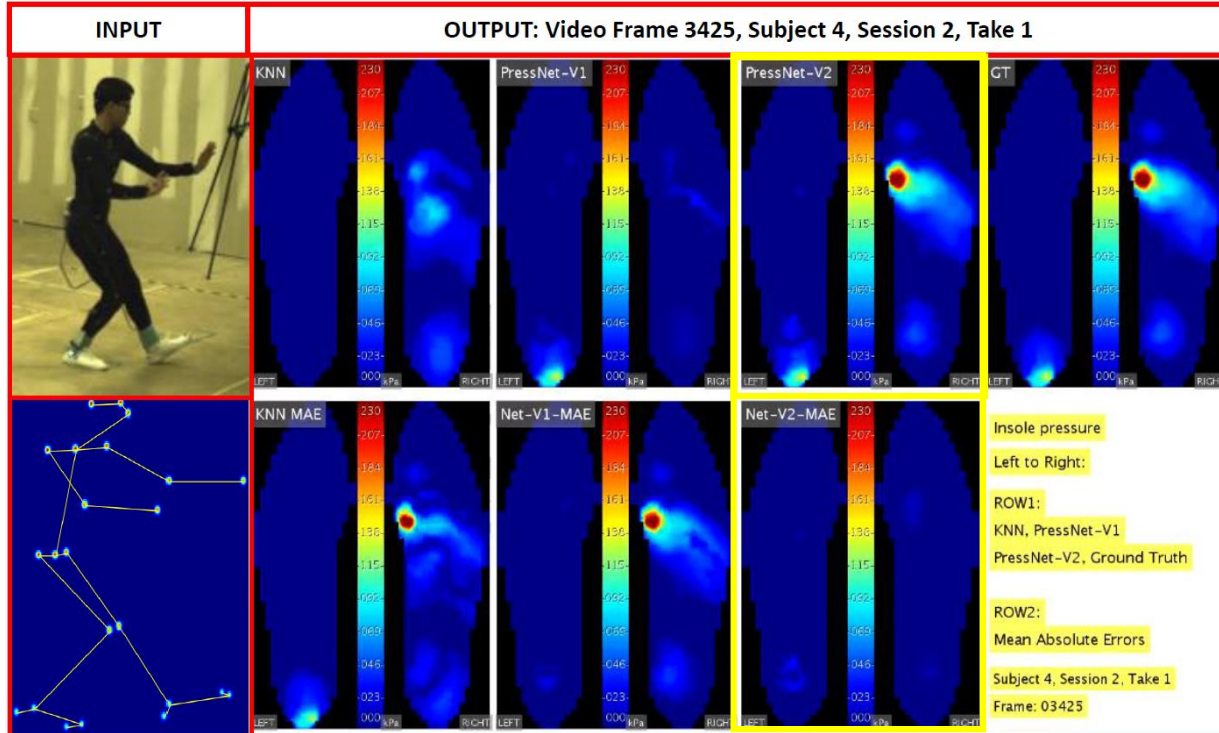


Figure 5: Qualitative results showing (Left to Right): Input data, Video Frame 3425 from Subject 4, Session 2, Take 1. The best prediction has a yellow bounding box around it.

and 12153 of Subject 10, Session 2, Take 1 (last row). They have similar foot pressure heatmaps, with the left heel and the right fore foot having a high pressure intensity, but they correspond to two different poses from two different subjects, the poses from the front view of Subject4 and side view of Subject 10. It can be clearly seen from visualization that PressNET-V2 generates heatmaps with similar pressure intensities as ground truth for both the frames. This shows that our network is able to capture the correlation between joint locations and foot pressure, irrespective of subject, pose, or camera view. Subjects 7 and 9 show the same response, suggesting that our network is not susceptible to changes in gender, even with different body dynamics and styles.

It can be observed that for Subject 10 in Figure 4, KNN performs better than PressNET. One of the reasons for this might be that the KNN finds a similar pose with a similar foot pressure map in the training data, since multiple poses can lead to the same foot pressure. This frame captures a side view with occluded limbs. Four OpenPose joints have zero confidences, leading to a worse mean absolute error on PressNET-V1 and PressNET-V2.

Figures 5, 7, 8 and 9 each show a sample result along with the corresponding input Tai Chi video frames and open pose joint heatmaps for subjects 4, 8, 9 and 10 respectively. Each figure has 8 sub-frames. Sub-frames in row 1, from left to right, portray predictions from KNN, PressNET-V1,

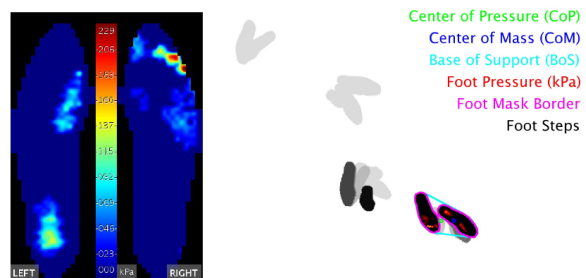


Figure 6: Example frame from Subject 4, Session 1, Take 2. **Left:** both left and right foot pressure maps, color coded by pressure (kPa); **Right:** a foot pressure sequence spatiotemporally registered to the motion capture coordinate system. PressNET-V2 and Ground Truths. Under each prediction, in row 2, is the corresponding absolute difference heatmap with respect to ground truth foot pressure. The last sub-frame in row 2 provides information about the video frame. Best prediction in each sample has a yellow bounding box around it.

## 5. Center of Pressure and Stability

Human gait stability analysis provides an overall motivation for our work. Stability analysis seeks to understand complex mechanisms of the human postural system that contribute to the development of efficient solutions for unstable postures in terms of orientation and equilibrium [5, 14, 18, 42, 45, 53].



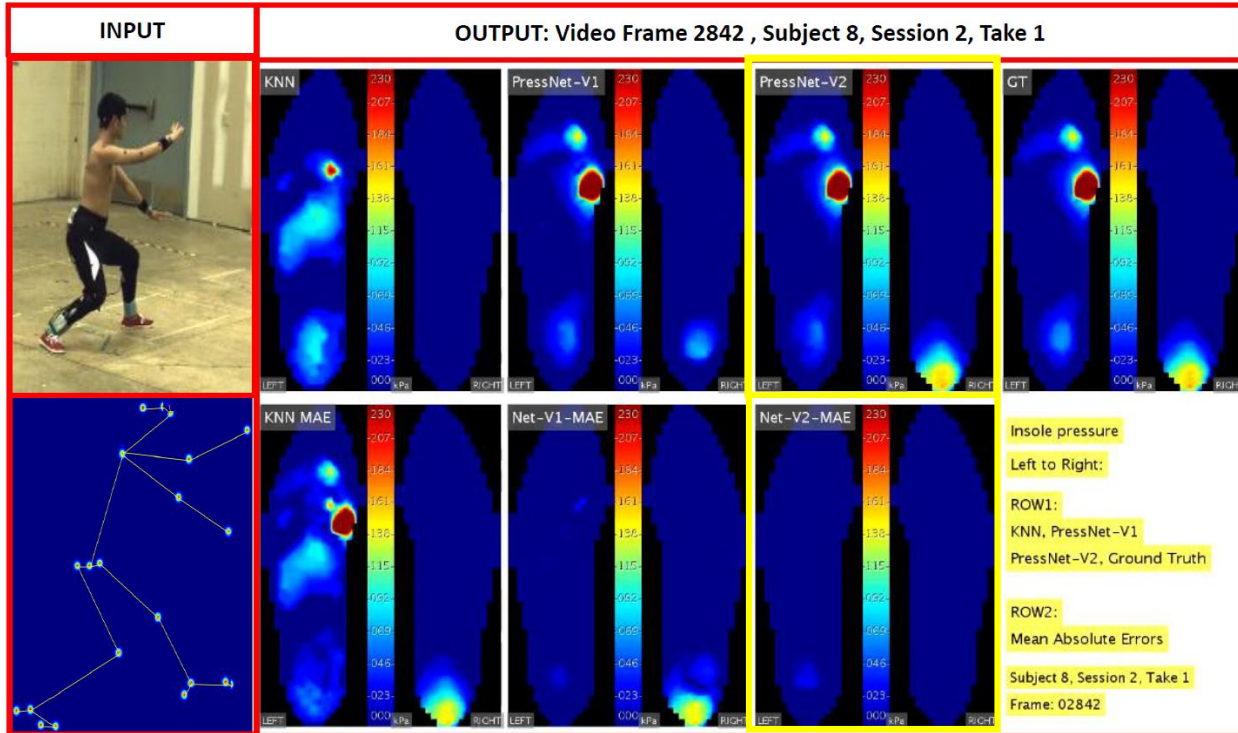


Figure 7: Qualitative results showing (Left to Right): Input data, Video Frame 2842 from Subject 8, Session 2, Take 1. The best prediction has a yellow bounding box around it.

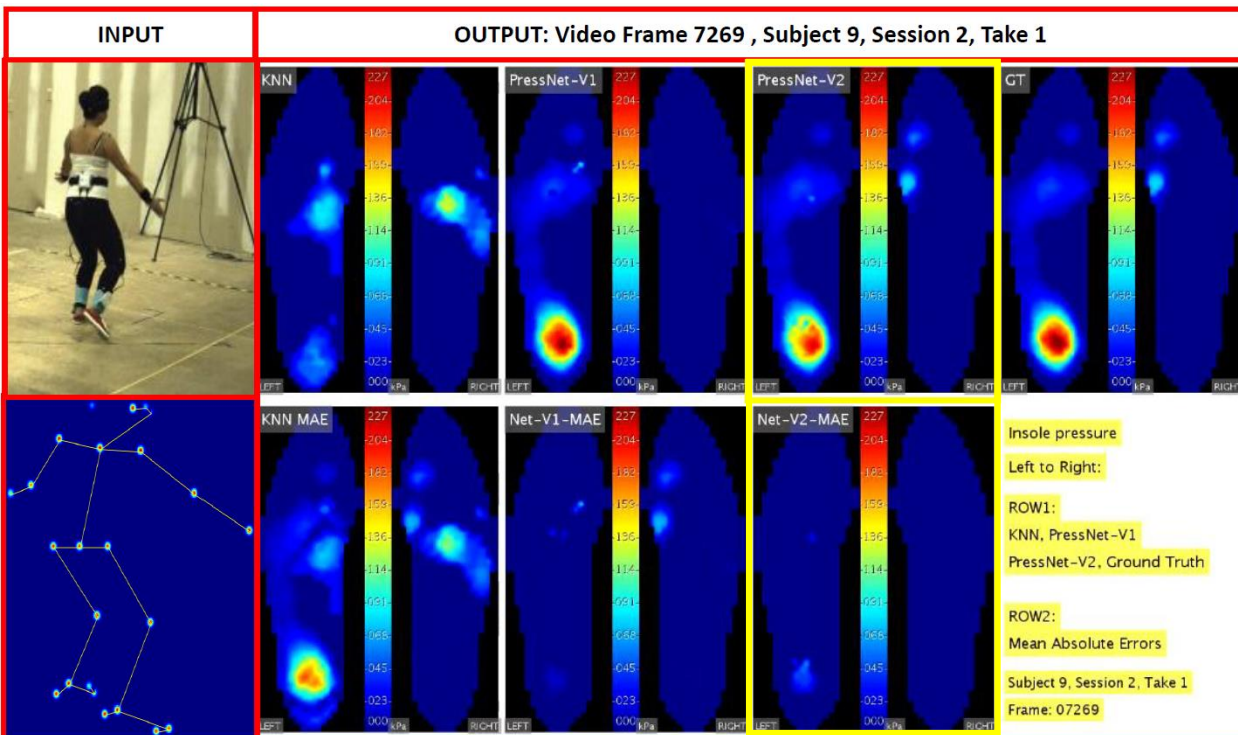


Figure 8: Qualitative results showing (Left to Right): Input data, Video Frame 7269 from Subject 9, Session 2, Take 1. The best prediction has a yellow bounding box around it.

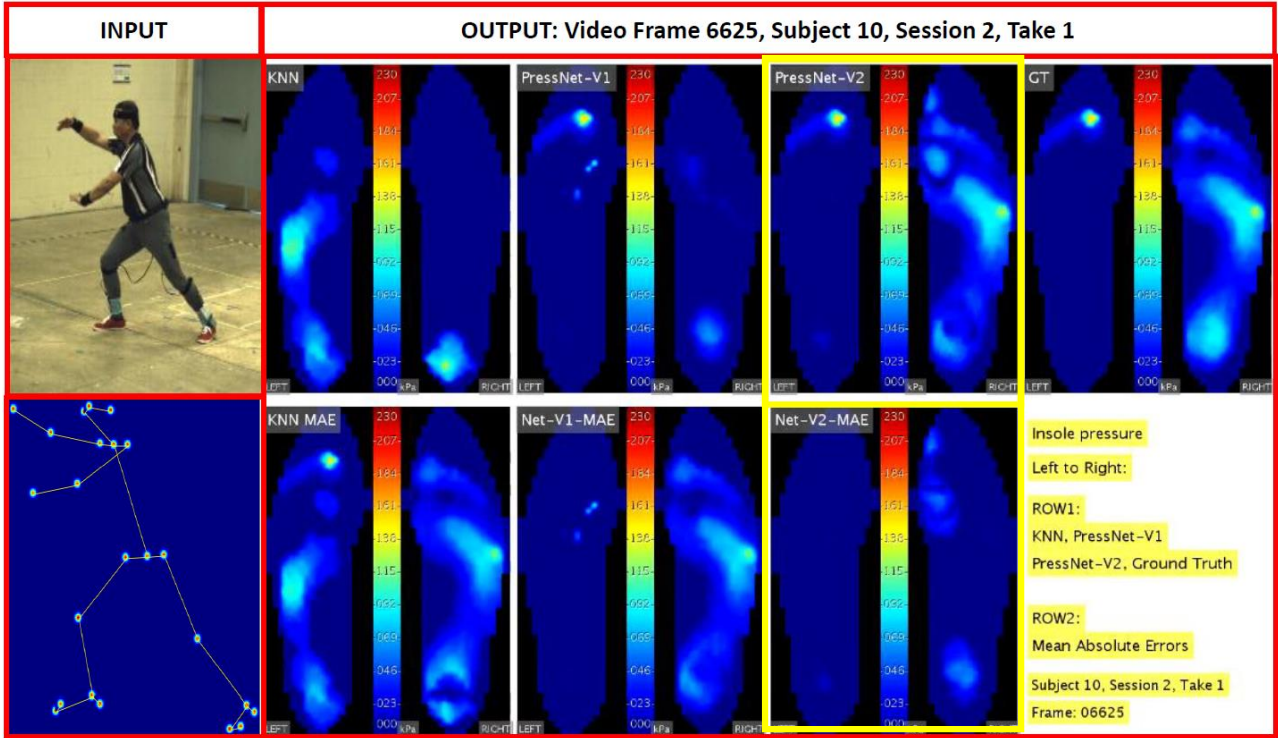


Figure 9: Qualitative results showing (Left to Right): Input data, Video Frame 6625 from Subject 10, Session 2, Take 1. The best prediction has a yellow bounding box around it.

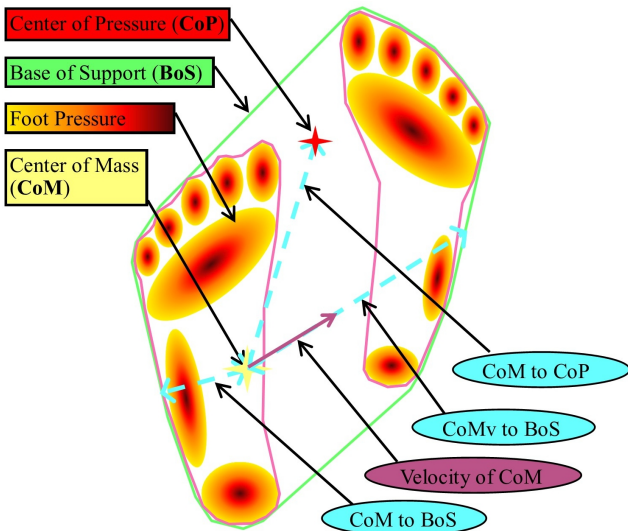


Figure 10: Stability Components

### 5.1. Background Concepts in Stability

Several fundamental concepts used in stability analysis are illustrated in Figures 6 and 10, including Center of Mass (CoM), Base of Support (BoS), and Center of Pressure (CoP) [50]. CoM, also known as Center of Gravity, is the ground projection of the body’s 3D center of mass onto the Base of Support (BoS) [21]. A human gait is stable

if the CoM falls within BoS, also called the support polygon [33]. If the CoM point is outside the support polygon, it is equivalent to the presence of an uncompensated moment acting on the foot, which causes it to rotate around the point on the polygon boundary resulting in instability. Center of Pressure (CoP), also known as the Zero Moment Point, is a point where the total moment generated due to gravity and inertia equals zero. Figure 10 shows a diagram of foot pressure annotated with the CoP, shown as a red star, relative to the pressure from both feet shown as regions color-coded from low pressure (yellow) to moderate pressure (red) to high pressure (brown). Considering CoP as the ground reaction force and CoM as the opposing force, larger distances between the two 2D points could indicate reduced stability. Indeed, the CoP location relative to the whole body center of mass has been identified as a determinant of stability in a variety of tasks [24, 25, 37]. Note that the CoP is usually measured directly by force plates or insole foot pressure sensors, whereas in this section we are evaluating our ability to infer it from video alone.

### 5.2. Quantitative Evaluation of Estimated CoP

As a step towards analyzing gait stability from video, in this section we compute Center of Pressure, one of the key components of stability, from the regressed foot pressure maps produced by our PressNET-V2 network, and compare it to CoP computed from the KNN baseline as well as from

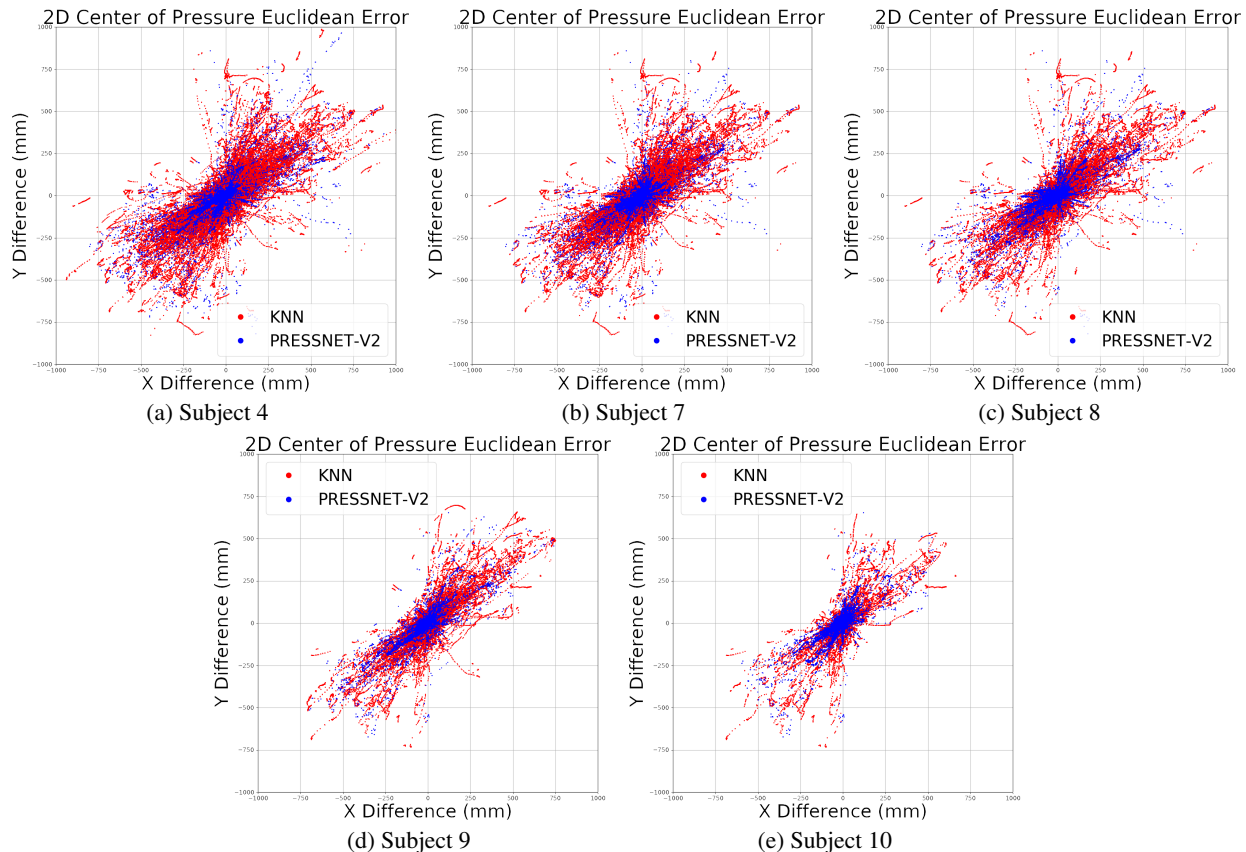


Figure 11: The 2D center of pressure euclidean error plots for KNN and PressNET-V2 on each subject.

the ground truth pressure data. For each of these types of foot pressure map, CoP is calculated as the weighted mean of the pressure elements (prexels) in the XY ground plane. The square root of mean squared error distance metric is chosen to calculate the 2D error between ground truth and our models. Table 5 lists the distance errors of CoP for KNN and PressNET-V2. PressNET-V2 has significantly lower errors for all subjects, making it a better tool for human gait stability analysis. Figure 11 shows the 2D CoP distance errors for Subjects 4, 7, 8, 9 and 10. It can be observed from the figures that the spread of errors of CoP is significantly lower compared to that of KNN.

From Table 5, it is evident that the median errors for PressNET-V2 are approximately 3 times smaller than that of KNN. The distribution of distance errors are concentrated around zero millimeters, showing that the accuracy of CoP calculations are significantly better than KNN, with smaller variance. As a point of reference, we know from [51] that a CoM accurate to 1% of the subject’s height (18mm) is as accurate as the variation between multiple CoM calculation methods. This can be used as an order of magnitude approximation of how accurate a video based method would expected to be for approximating CoP. We believe this is a promising result towards developing a deep learning framework for human gait stability analysis from video.

KNN		2D CoP Euclidean Error (mm)			
Test Subject	Mean	Std	Median	Max	Min
4	196.87	198.83	<b>122.93</b>	1136.4	0
7	163.97	157.94	<b>103</b>	699.76	0
8	216.16	222.78	<b>123.61</b>	1067	0
9	191.56	200.92	<b>111.36</b>	902.73	0
10	179.1	173.1	<b>116.98</b>	971.52	0

PressNET V2		2D CoP Euclidean Error(mm)			
Test Subject	Mean	Std	Median	Max	Min
4	66.18	116.78	<b>26.51</b>	1179	0
7	52.36	83.64	<b>23.09</b>	682.72	0
8	70.98	119.9	<b>30.59</b>	1048.1	0
9	61.83	109.9	<b>20.76</b>	888.11	0
10	59.25	95.67	<b>25.51</b>	759.82	0

Table 5: CoP Distance Error (root mean squared distance from Ground Truth) for KNN and PressNET-V2. PressNET errors are on an order of magnitude lower than the KNN baseline.

## 6. Summary and Conclusion

In this paper, we explore the feasibility of regressing foot pressure from 2D joint detected in video. This is the first work in an effort to bring a direct mapping from whole human body kinematics to foot pressure dynamics into the

computer vision community. We demonstrate, both quantitatively and qualitatively the effectiveness of our PressNET networks on a challenging, long, multimodality Taiji performance dataset. We demonstrate statistically significant improved results over a standard K-Nearest Neighbor method, to validate that our networks are indeed learning foot pressures from body kinematics. We also demonstrate the use of learned foot pressure for estimation of *Center of Pressure*, a key component of postural and gait stability, from the regressed foot pressure results.

We hope to extend this work to integrate additional body dynamics to allow accurate modeling of forces, dynamics and stability exclusively from video. Our goal is to build *precision computer vision* tools that estimate various human body dynamics using passive and inexpensive visual sensors, whose outcome is validated using bio-mechanically derived data (rather than approximations by human labelers). We foresee to introduce a new and exciting sub-field in computer vision beyond visually satisfactory human joint/pose detection to the more challenging problems of capturing accurate, quantifiable human body dynamics for scientific applications.

## 7. Acknowledgments

We would like to thank all the anonymous human volunteers who contributed their 24-form Taiji performances to this study. We would like to acknowledge Andy Lou for his help in rendering the images and videos for demonstration. We thank the College of Engineering dean's office of Penn State University for supporting our motion capture lab for research and education. This work is supported in part by NSF grant IIS-1218729.

## References

- [1] A. Agarwal and B. Triggs. 3d human pose from silhouettes by relevance vector regression. In *Computer Vision and Pattern Recognition, 2004. CVPR 2004. Proceedings of the 2004 IEEE Computer Society Conference on*, volume 2, pages II–II. IEEE, 2004. 2
- [2] S. J. Allen, M. A. King, and M. R. Yeadon. Is a single or double arm technique more advantageous in triple jumping? *Journal of Biomechanics*, 43(15):3156–3161, 2011. 2
- [3] R. Alp Güler, N. Neverova, and I. Kokkinos. Densepose: Dense human pose estimation in the wild. In *The IEEE Conference on Computer Vision and Pattern Recognition (CVPR)*, June 2018. 1, 2
- [4] M. Arvin, M. Hoozemans, M. Pijnappels, J. Duysens, S. M. P. Verschueren, and J. Van Dieen. Where to step? contributions of stance leg muscle spindle afference to planning of mediolateral foot placement for balance control in young and older adults. *Frontiers in Physiology*, 9:1134, 2018. 3
- [5] S. J. M. Bamberg, A. Y. Benbasat, D. M. Scarborough, D. E. Krebs, and J. A. Paradiso. Gait analysis using a shoe-integrated wireless sensor system. *IEEE Transactions on Information Technology in Biomedicine*, 12(4):413–423, 2008. 8
- [6] C. M. Bishop. *Pattern Recognition and Machine Learning (Information Science and Statistics)*. Springer-Verlag, Berlin, Heidelberg, 2006. 5
- [7] F. Bogo, A. Kanazawa, C. Lassner, P. Gehler, J. Romero, and M. J. Black. Keep it smpl: Automatic estimation of 3d human pose and shape from a single image. In *European Conference on Computer Vision*, pages 561–578. Springer, 2016. 2
- [8] A. Bulat and G. Tzimiropoulos. Human pose estimation via convolutional part heatmap regression. In *European Conference on Computer Vision*, pages 717–732. Springer, 2016. 1, 2
- [9] Z. Cao, T. Simon, S.-E. Wei, and Y. Sheikh. Realtime multi-person 2d pose estimation using part affinity fields. In *The IEEE Conference on Computer Vision and Pattern Recognition (CVPR)*, volume 1, page 7, 2017. 1, 2, 3
- [10] C.-H. Chen and D. Ramanan. 3d human pose estimation= 2d pose estimation+ matching. In *The IEEE Conference on Computer Vision and Pattern Recognition (CVPR)*, volume 2, page 6, 2017. 2
- [11] W. Chen, H. Wang, Y. Li, H. Su, Z. Wang, C. Tu, D. Lischinski, D. Cohen-Or, and B. Chen. Synthesizing training images for boosting human 3d pose estimation. In *3D Vision (3DV), 2016 Fourth International Conference on*, pages 479–488. IEEE, 2016. 1, 2
- [12] X. Chen and A. L. Yuille. Articulated pose estimation by a graphical model with image dependent pairwise relations. In *Advances in Neural Information Processing Systems (NIPS)*, pages 1736–1744, 2014. 1, 2
- [13] F. Chollet. Xception: Deep learning with depthwise separable convolutions. In *The IEEE Conference on Computer Vision and Pattern Recognition (CVPR)*, July 2017. 5
- [14] S. H. Collins and A. Ruina. A bipedal walking robot with efficient and human-like gait. In *Robotics and Automation, 2005. ICRA 2005. Proceedings of the 2005 IEEE International Conference on*, pages 1983–1988. IEEE, 2005. 8
- [15] Z. J. Domire and J. H. Challis. Maximum height and minimum time vertical jumping. *Journal of Biomechanics*, 48(11):2865–2870, 2015. 2
- [16] N. Eckardt and N. J. Rosenblatt. Healthy aging does not impair lower extremity motor flexibility while walking across an uneven surface. *Human Movement Science*, 62:67–80, 2018. 3
- [17] X. Fan, K. Zheng, Y. Lin, and S. Wang. Combining local appearance and holistic view: Dual-source deep neural networks for human pose estimation. In *Proceedings of the IEEE Conference on Computer Vision and Pattern Recognition*, pages 1347–1355, 2015. 1, 2
- [18] A. Gefen, M. Megido-Ravid, Y. Itzchak, and M. Arcan. Analysis of muscular fatigue and foot stability during high-heeled gait. *Gait & posture*, 15(1):56–63, 2002. 8
- [19] A. Gilbert, M. Trumble, C. Malleson, A. Hilton, and J. Colomosse. Fusing visual and inertial sensors with semantics for 3d human pose estimation. *International Journal of Computer Vision*, pages 1–17, 2018. 2
- [20] S. R. Goldberg, S. Ounpuu, and S. L. Delp. The importance of swing-phase initial conditions in stiff-knee gait. *Journal*

- of *Biomechanics*, 36(8):1111–1116, 2003. 2
- [21] A. Goswami. Foot rotation indicator (fri) point: a new gait planning tool to evaluate postural stability of biped robots. In *Proceedings 1999 IEEE International Conference on Robotics and Automation (Cat. No.99CH36288C)*, volume 1, pages 47–52 vol.1, May 1999. 10
- [22] R. Grimm, J. Sukkau, J. Hornegger, and G. Greiner. Automatic patient pose estimation using pressure sensing mattresses. In *Bildverarbeitung für die Medizin 2011*, pages 409–413. Springer, 2011. 3
- [23] I. Gulrajani, F. Ahmed, M. Arjovsky, V. Dumoulin, and A. C. Courville. Improved training of wasserstein gans. In *Advances in Neural Information Processing Systems*, pages 5767–5777, 2017. 4
- [24] A. L. Hof. The equations of motion for a standing human reveal three mechanisms for balance. *Journal of Biomechanics*, 40(2):451–457, 2007. 10
- [25] A. L. Hof. The ‘extrapolated center of mass’ concept suggests a simple control of balance in walking. *Human Movement Science*, 27(1):112–125, 2008. 10
- [26] G. Huang, Z. Liu, L. Van Der Maaten, and K. Q. Weinberger. Densely connected convolutional networks. In *The IEEE Conference on Computer Vision and Pattern Recognition (CVPR)*, volume 1, page 3, 2017. 2
- [27] M. A. Hughes, B. S. Myers, and M. L. Schenkman. The role of strength in rising from a chair in the functionally impaired elderly. *Journal of Biomechanics*, 29(12):1509–1513, 1996. 2
- [28] S. Ioffe and C. Szegedy. Batch normalization: Accelerating deep network training by reducing internal covariate shift. In *Proceedings of the 32Nd International Conference on International Conference on Machine Learning - Volume 37, ICML’15*, pages 448–456. JMLR.org, 2015. 5
- [29] E. D. Lemaire, A. Biswas, and J. Kofman. Plantar pressure parameters for dynamic gait stability analysis. In *Engineering in Medicine and Biology Society, 2006. EMBS’06. 28th Annual International Conference of the IEEE*, pages 4465–4468. IEEE, 2006. 3
- [30] Y. Liu, R. Collins, and Y. Tsin. Gait sequence analysis using frieze patterns. In *European Conference on Computer Vision*, pages 657–671. Springer, 2002. 3
- [31] J. Martinez, R. Hossain, J. Romero, and J. J. Little. A simple yet effective baseline for 3d human pose estimation. In *IEEE International Conference on Computer Vision*, volume 206, page 3, 2017. 2
- [32] F. Moreno-Noguer. 3d human pose estimation from a single image via distance matrix regression. In *2017 IEEE Conference on Computer Vision and Pattern Recognition (CVPR)*, pages 1561–1570. IEEE, 2017. 2
- [33] J. Mrozowski, J. Awrejcewicz, and P. Bammerski. Analysis of stability of the human gait. *Journal of Theoretical and Applied Mechanics*, 45(1):91–98, 2007. 10
- [34] V. Nair and G. E. Hinton. Rectified linear units improve restricted boltzmann machines. In *Proceedings of the 27th International Conference on Machine Learning (ICML-10)*, pages 807–814, 2010. 5
- [35] A. Newell, K. Yang, and J. Deng. Stacked hourglass networks for human pose estimation. In *European Conference on Computer Vision*, pages 483–499. Springer, 2016. 1, 2
- [36] B. X. Nie, P. Wei, and S.-C. Zhu. Monocular 3d human pose estimation by predicting depth on joints. In *IEEE International Conference on Computer Vision*, 2017. 2
- [37] Y.-C. Pai. Movement termination and stability in standing. *Exercise and Sport Sciences Reviews*, 31(1):19–25, 2003. 10
- [38] G. Pavlakos, X. Zhou, K. G. Derpanis, and K. Daniilidis. Coarse-to-fine volumetric prediction for single-image 3d human pose. In *Computer Vision and Pattern Recognition (CVPR), 2017 IEEE Conference on*, pages 1263–1272. IEEE, 2017. 2
- [39] J. Perry, J. R. Davids, et al. Gait analysis: normal and pathological function. *Journal of Pediatric Orthopaedics*, 12(6):815, 1992. 1
- [40] R. J. Peterka and P. J. Loughlin. Dynamic regulation of sensorimotor integration in human postural control. *Journal of neurophysiology*, 91(1):410–423, 2004. 1
- [41] G. Rogez, P. Weinzaepfel, and C. Schmid. Lcr-net++: Multi-person 2d and 3d pose detection in natural images. *CoRR*, abs/1803.00455, 2018. 2
- [42] L. Shu, T. Hua, Y. Wang, Q. Li, D. D. Feng, and X. Tao. In-shoe plantar pressure measurement and analysis system based on fabric pressure sensing array. *IEEE Transactions on Information Technology in Biomedicine*, 14(3):767–775, 2010. 8
- [43] E. Simo-Serra, A. Ramisa, G. Alenyà, C. Torras, and F. Moreno-Noguer. Single image 3d human pose estimation from noisy observations. In *Computer Vision and Pattern Recognition (CVPR), 2012 IEEE Conference on*, pages 2673–2680. IEEE, 2012. 2
- [44] X. Sun, J. Shang, S. Liang, and Y. Wei. Compositional human pose regression. In *The IEEE International Conference on Computer Vision (ICCV)*, volume 2, 2017. 2
- [45] W. Tao, T. Liu, R. Zheng, and H. Feng. Gait analysis using wearable sensors. *Sensors*, 12(2):2255–2283, 2012. 8
- [46] D. Tomè, C. Russell, and L. Agapito. Lifting from the deep: Convolutional 3d pose estimation from a single image. *The IEEE Conference on Computer Vision and Pattern Recognition (CVPR)*, pages 2500–2509, 2017. 2
- [47] J. Tompson, R. Goroshin, A. Jain, Y. LeCun, and C. Bregler. Efficient object localization using convolutional networks. In *Proceedings of the IEEE Conference on Computer Vision and Pattern Recognition*, pages 648–656, 2015. 5
- [48] J. A. L. Y. B. C. Tompson, J.J. Joint training of a convolutional network and a graphical model for human pose estimation. In: *Advances in Neural Information Processing Systems. (2014) 17991807*. 2
- [49] A. Toshev and C. Szegedy. Deeppose: Human pose estimation via deep neural networks. In *Proceedings of the IEEE Conference on Computer Vision and Pattern Recognition*, pages 1653–1660, 2014. 1, 2
- [50] M. Virnavirta and J. Isolehto. Determining the location of the body’s center of mass for different groups of physically active people. *Journal of Biomechanics*, 47(8):1909–1913, 2014. 10
- [51] M. Virnavirta and J. Isolehto. Determining the location of the body’s center of mass for different groups of physically active people. *Journal of Biomechanics*, 47(8):1909–1913, jun 2014. 11
- [52] C. Wang, R. Bannuru, J. Ramel, B. Kupelnick, T. Scott, and

- C. Schmid. Tai chi on psychological well-being: systematic review and meta-analysis. *BMC complementary and alternative medicine*, pages 10–23, 2010. [2](#)
- [53] M. W. Whittle. Gait analysis. In *The Soft Tissues*, pages 187–199. Elsevier, 1993. [8](#)
- [54] D. A. Winter. *Biomechanics and motor control of human gait: normal, elderly and pathological*. 1991. [1](#)
- [55] X. Zhou, Q. Huang, X. Sun, X. Xue, and Y. Wei. Towards 3d human pose estimation in the wild: a weakly-supervised approach. In *IEEE International Conference on Computer Vision*, 2017. [2](#)
- [56] X. Zhou, M. Zhu, S. Leonardos, K. G. Derpanis, and K. Daniilidis. Sparseness meets deepness: 3d human pose estimation from monocular video. In *Proceedings of the IEEE Conference on Computer Vision and Pattern Recognition*, pages 4966–4975, 2016. [2](#)